Journal of Applied Physics

RESEARCH ARTICLE | MARCH 24 2022

Tuning the feature size of nanoimprinting stamps: A method to enhance the flexibility of nanoimprint lithography

Matthias Golibrzuch ; Thomas L. Maier ; Moritz J. Feil ; Katharina Krischer ; Markus Becherer

J. Appl. Phys. 131, 124301 (2022)
https://doi.org/10.1063/5.0079282

16 April 2024 08:25:33

Journal of Applied Physics ARTICLE scitation.org/journal/jap

Tuning the feature size of nanoimprinting stamps: A method to enhance the flexibility of nanoimprint lithography

Cite as: J. Appl. Phys. **131**, 124301 (2022); doi: 10.1063/5.0079282
Submitted: 19 November 2021 · Accepted: 9 March 2022 ·
Published Online: 24 March 2022

View Online

Export Citation

CrossMark

Matthias Golibrzuch,[1,a)] Thomas L. Maier,[2] Moritz J. Feil,[2] Katharina Krischer,[2] and Markus Becherer[1]

AFFILIATIONS

[1]Chair of Nano and Quantum Sensors, Department of Electrical and Computer Engineering, Technical University of Munich, 85748 Garching, Germany
[2]Nonequilibrium Chemical Physics, Department of Physics, Technical University of Munich, 85748 Garching, Germany

[a)]**Author to whom correspondence should be addressed:** matthias.golibrzuch@tum.de

ABSTRACT

In the field of nanoimprinting lithography, fabricating large-area imprinting stamps is often the most time- and resource-consuming step. Specifically in research, it is often not reasonable to produce a new imprinting stamp for each new experimental configuration. Therefore, the lack of flexibility in feature sizes makes prototyping and tailoring the feature sizes according to their application challenging. To overcome these restrictions, we developed an imprinting stamp reproduction and tuning method which enables the size of the features of existing imprinting stamps to be tuned within nanometer precision. For replication, we first fabricate a chromium nanoisland array on silicon dioxide using the to-be tuned imprinting stamp. Then, the silicon dioxide is anisotropically etched in a reactive ion etching process with chromium as a hard mask. The formed replica of the imprinting stamp is subsequently tuned in an isotropic etching step with hydrofluoric acid. The method enables us to tune the size of the features of our nanoimprinting stamps within nanometer precision without influencing their shape with a yield above 96%. The tuned stamps are then used to fabricate metal nanoisland arrays with the respective tuned sizes. To evaluate the influence of the feature sizes, we exemplarily study the plasmonic resonance of gold nanoisland arrays fabricated using stamps with different feature diameters. Here, we see a good agreement between measured and simulated plasmonic resonance wavelengths of the samples. Hence, with the tuning method, we can tailor specific size-dependent properties of our nanoisland arrays according to individual experiments and applications.

© 2022 Author(s). All article content, except where otherwise noted, is licensed under a Creative Commons Attribution (CC BY) license (http://creativecommons.org/licenses/by/4.0/). https://doi.org/10.1063/5.0079282

16 April 2024 08:25:33

I. INTRODUCTION

Since its first applications almost 30 years ago,[1,2] nanoimprint lithography (NIL) proved vital as a nanopatterning technique in research.[3,4] Nanoimprinted structures found several applications, among others in plasmonics,[5,6] in electrochemistry,[7,8] or for solar cells.[9,10] The ability to fabricate nanostructures over large areas in a cheap, fast, and reliable process[11] makes NIL favorable compared to other nanopatterning methods, such as optical and e-beam lithography. NIL enables the production of structures of a few nanometers with nanometer precision.[12] As optical lithography with binary masks is diffraction limited to a feature size of minimum $\lambda/2$, where λ is the optical wavelength, very short wavelengths in the extreme ultraviolet (EUV) regime must be used to produce feature sizes comparable to NIL processes.[13] Optical lithography devices using EUV light are expensive and optimized for industrial purposes and, therefore, not appropriate for research. Electron beam lithography is able to produce nanostructures on the same length scales as NIL;[14] however, electron beam lithography lacks the ability of non-linear scaling of the area to be structured. Contrarily, NIL allows fast patterning in the nanometer regime over areas up to several square centimeters[15] and wafer scale[16] once an imprinting mold is produced. Hence, in the past, the imprinting stamp fabrication process often was the bottle neck in NIL fabrication processes. Several methods to fabricate imprinting stamps emerged, such as e-beam lithography,[6,8,12] interference lithography,[17–19] optical

© Author(s) 2022

projection lithography,[9] or by using block co-polymers.[20,21] E-beam lithography provides the most flexibility to create the desired patterns. However, e-beam lithography is the most time- and resource-consuming method. Nevertheless, we experience that, once finished, an imprinting stamp can function as a template for several hundred of copies over ten years.

A disadvantage of NIL that comes with the resource-consuming imprinting stamp production process is the lack of structural versatility after the imprinting stamp is fabricated. The features of the fabricated imprinting stamp are fixed, and due to the elaborate fabrication process, it is not favorable to produce an imprinting stamp for each individual experiment. Hence, the dimensions of the nanostructures fabricated with NIL are, in principle, determined during the fabrication of the imprinting stamp. However, in the applications of NIL-fabricated nanoisland arrays, the size of the individual nanoislands often plays an important role.[6,8] Specifically for applications utilizing light–matter interactions, the lateral dimensions of the nanoislands determine the resonant wavelengths for the occurring interactions between incoming light and the nanoislands. For example, in plasmonic applications, the dimensions of metal nanoislands in a nanoimprinted array have great influence on the plasmonic properties of the nanoislands.[5,22,23] Specifically, the plasmonic resonance wavelength is dependent on the lateral dimensions of the nanoislands.[6] Hence, the size of the nanoimprinted nanoislands influences whether a plasmonic device works, for example, in the visible or infrared regime. Therefore, the ability to tune the feature sizes of nanoimprinted nanoisland arrays can unfold new possibilities to adjust the working regime of plasmonic devices.

There are two different approaches to tune the sizes of the NIL-fabricated nanostructures. Either the imprinting stamp itself is tuned (stamp tuning) or the nanopatterned resist is manipulated after the imprinting process (resist tuning). Resist tuning is performed, for example, by using V-shaped imprinting stamps where anisotropic etching of the resist increases the width of the fabricated lines,[19] by imprinting in a combination with angeled evaporation to decrease the width of grating lines,[24] or by isotropically widening imprinted holes in a resist to increase the size of imprinted nanoislands.[6] The advantage of the resist tuning approach is versatility and adaptability during the process. The disadvantages of the resist tuning approach are the complexity of the process and that resist tuning techniques only allow to remove resist in the process; hence, it allows just to increase holes or grooves in the resist. Therefore, the feature sizes of the final NIL structures can only be tuned larger when using a lift-off process or they can only be tuned smaller, when using an etching process. Other than that, with stamp tuning, it is possible to tune the size of the stamp features directly and with that the final imprinted structures both smaller and larger independent of the later imprinting process. To decrease the feature size, the imprinting mold is isotropically etched.[10] To increase the feature size, the stamp is isotropically coated with a suitable coating.[25] Additionally, laser melting allows to reshape the features of a stamp[26] or multi-stack imprinting allows to fabricate stamps with a combination of features of the used stamps.[27] The advantage of the stamp tuning approach is the enhanced reproducibility of samples compared to resist tuning, as one tuned stamp functions as template for all samples of one size produced with NIL. Furthermore, once tuned, the stamp can be used in all established imprinting methods and no more complex procedures must be applied. The disadvantage of the stamp tuning approach is that the original stamp itself is altered and the original pattern is lost. Hence, to preserve the original stamp, a replica has to be fabricated before the tuning process.

In this work, we apply the stamp tuning approach to tune the feature sizes of large area $5 \times 5\,\mathrm{mm}^2$ e-beam fabricated imprinting stamps for the fabrication of metal nanoisland arrays. We present a non-linear scalable method to stepless tune the feature sizes of nanoimprinting stamps without the need of complex equipment in a cost-effective and simple process. Therefore, we first fabricate a replica of our original imprinting stamp and perform the stamp tuning process on the replicated stamp. We use a double-layer resist lift-off nanoimprint lithography (LO-NIL)[6] to fabricate a chromium nanoisland array, which is used as a hard mask for anisotropic dry etching of the substrate material to transfer the features of the stamp into the replica.[20] We opted for silicon dioxide (SiO_2) as the material of choice for the reproduced stamps. SiO_2 can be deposited or grown on silicon substrates in high quality, and at the same time, it can be isotropically etched by hydrofluoric acid (HF) in a controlled and selective way. We use this property of SiO_2 to tune the feature sizes of the replicated stamps. Once the stamps are tuned to the desired size, we can fabricate metal nanoisland arrays using the same double-layer resist LO-NIL process with the replicated and tuned stamps. The newly fabricated metal nanoisland arrays exhibit altered plasmonic properties due to their different feature sizes. Thus, we can engineer the plasmonic properties of the metal nanoisland arrays according to their desired application.

II. RESULTS AND DISCUSSION

To allow changing the size of nanoimprinted features without the need to produce a new imprinting stamp, we developed a process to reproduce and subsequently tune an existing large-area imprinting stamp. In the following, we first present the reproduction and tuning method and review the proposed processes. Next, we show the implementation of the method by tuning imprinting stamps to different feature sizes and use these tuned stamps to fabricate gold nanoisland arrays. Furthermore, as example application, we investigate the influence of the feature size tuning on the plasmonic properties of the gold nanoisland arrays and compare the results with our simulations.

A. Imprinting stamp reproduction and tuning method

In all our imprinting processes, we use commercially fabricated silicon imprinting stamps further referred to as original stamps, which are fabricated via electron beam lithography. To prevent the original stamps from damage, we are not using them directly for our imprinting processes. Instead, we use the original stamps as templates for semi-flexible single-use stamps (working stamps).[28,29] These working stamps are not tuneable, neither via dry nor wet etching techniques. Hence, to tune the dimensions of the imprinting stamp and preserve the original stamp, we first need to reproduce the original stamp in a material that can be etched isotropically, which enables a tuning process. Our material of

16 April 2024 08:25:33

© Author(s) 2022

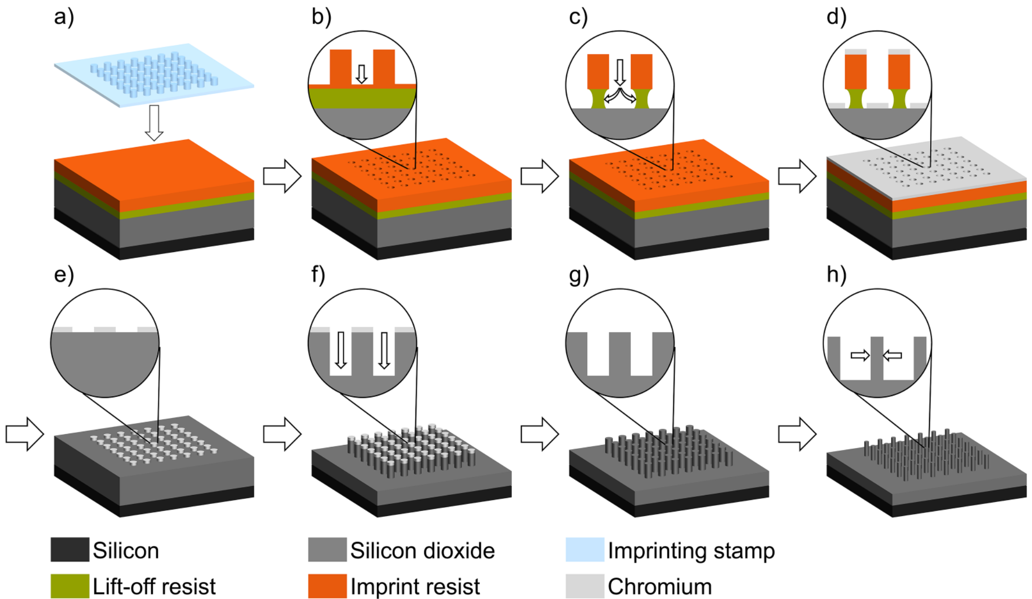

FIG. 1. Schematic depiction of the imprinting stamp replication and tuning process consisting of the three process phases: (a)–(e) double resist LO-NIL of chromium nano-islands, (e)–(g) dry etching to form a SiO_2 replica stamp, and (g)–(h) HF tuning of the stamp features. (a) The lift-off resist (green) and the imprint resist (orange) are spin-coated onto the SiO_2 surface before the imprinting mold is applied to the sample. (b) The actual imprinting process transfers the features of the imprinting stamp into the imprint resist. The inset shows the inevitable residual layer of the imprint resist. (c) The residual layer is removed via an anisotropic dry etching step, followed by an isotropic wet etching step of the lift-off resist to expose the SiO_2 surface and to create an artificial undercut. (d) Subsequently, chromium is evaporated onto the sample. (e) After lift-off, the chromium nano-island array remains on the SiO_2 surface. (f) In the following dry etching step, the chromium nanoislands are used as a hard mask to form pillars in the SiO_2 layer. (g) The chromium disks are removed. (h) The size of the pillars of the SiO_2 replica stamp is isotropically tuned in an HF acid based solution.

16 April 2024 08:25:33

choice is SiO_2. The use of diluted and buffered HF solution enables a slow and controlled isotropic etching process of SiO_2, which allows us to precisely tune the dimensions of the features of the reproduced stamps. However, first we reproduce the original stamp using a metal hard mask-assisted reactive ion etching (RIE) step, where a chromium hard mask is fabricated using our well-established LO-NIL process.[6] The whole reproduction and tuning process is schematically depicted in Fig. 1. For the LO-NIL process, we use a double-resist technique. For the double-resist layer NIL process, we first spincoat a lift-off resist and an imprinting resist on the silicon-SiO_2 substrate. Figure 1(a) shows the substrate after spincoating of the two resists. Next, we apply a working stamp with the desired features onto the sample and transfer the stamp-sample stack into an imprinter. In the imprinter, the sample is heated to above the imprint resists glass transition temperature. Hence, the thermo-viscous imprinting resist becomes viscous. Now, the working stamp is pressed into the imprint resist. During this process, the imprint resist fills the features of the working stamp. Hereby, the features of the stamp are transferred into the imprint resist. Before the demolding of the stamp, the sample is cooled to room temperature to harden the imprint resist. Then, the working stamp is mechanically removed from the imprint resist. Figure 1(b) illustrates the sample after the imprinting process; here, the inset shows a cross section through the sample. Now, a negative profile of the pattern of the working stamp is transferred into the imprint resist. However, the stamp always leaves a so-called residual layer in the imprint resist, a thin layer of resist on top of the underlying resist or the substrate. The residual layer is indicated by the arrow in the inset of Fig. 1(b). The residual layer must be removed in a RIE step to expose the lift-off resist for further processing. The inset in Fig. 1(c) shows the sample after the removal of the residual layer and the following developing step of the lift-off resist. We isotropically etch the exposed lift-off resist in a wet chemical development process. Hereby, we expose the SiO_2 surface for later metal evaporation and create an artificial undercut in the lift-off resist. The undercut ensures a smooth metal lift-off after the evaporation. In a next step, we evaporate chromium onto the sample. Figure 1(d) depicts the sample after the evaporation step. The artificial undercut prevents the deposition of chromium on the sidewalls of the lift-off resist, as can be seen in the inset of Fig. 1(d). Therefore, no metal bridges between the chromium on the SiO_2 surface and the chromium on top of the imprint resist can form. Hence, a smooth lift-off of the resists and the chromium on top is guaranteed. In a subsequent lift-off step, we remove both resists and the excess chromium on top of the resists. Figure 1(e) shows the sample after the lift-off process. The chromium nanoislands on top of the SiO_2 surface have the same diameters as the pillars of the original stamp and are inert to RIE gases used to etch SiO_2. Therefore, they are now used as a hard mask for an anisotropic RIE process to form pillars in the SiO_2 and reproduce the pattern of the original imprinting stamp, as depicted in Fig. 1(f). Subsequently, the chromium is selectively removed from the top of the pillars using a

© Author(s) 2022

chromium etchant. Figure 1(g) shows the SiO_2 reproduction of the original stamp after chromium removal. This reproduced stamp can be handled in the same way as the original stamp for all our NIL processes. The advantage of SiO_2 as the stamp material of the reproduced stamp compared to the original silicon stamp is that it can be isotropically etched by an HF-based solution in a controlled way. A slow etch rate of $0.2\,\mathrm{nm\,s^{-1}}$ allows us to precisely control the size of the tuned pillars and guarantees the conservation of the circular shape of the pillars during the tuning process. Thus, we can tune the diameter of the SiO_2 pillars without influencing their circular form. Hence, the final diameter of the pillars solely depends on the etching time in the HF solution. The final tuned SiO_2 stamp is illustrated in Fig. 1(h). Finally, we can use the tuned stamp for all our imprinting processes similarly to the original stamp.

B. Review of the reproduction and tuning process

To study the influence of the size of the metal nanoislands on our experiments, we use the stamp reproduction and tuning method described above to produce SiO_2 imprinting stamps with different feature sizes. Subsequently, we fabricated gold nanoisland arrays using these reproduced and tuned stamps and analyzed the influence of size tuning on the plasmonic properties of the gold nanoisland arrays. In this work, we focus on the reproduction and tuning of an original stamp with circular features with a nominal diameter of 75 nm over an area of 5 × 5 mm. The 75 nm circular features show light–matter interactions in the visible light regime and are, therefore, especially interesting for solar applications. Figure 2 shows a picture of the original stamp, a replicated and tuned stamp, and a gold nanoisland array fabricated with the tuned stamp. Each stamp and sample consists of about 10^{11} individual pillars or nanoislands.

To review our reproduction and tuning process, we took SEM images of the original stamp and SiO_2 stamps during the fabrication process. Figures 3(a)–3(d) show an SEM image of the original stamp, chromium nanoislands fabricated with the original stamp, a reproduced stamp, and a HF-tuned stamp, respectively. To further evaluate the shapes of the pillars of the original, the reproduced, and the tuned stamp, we took additional SEM images with a tilt

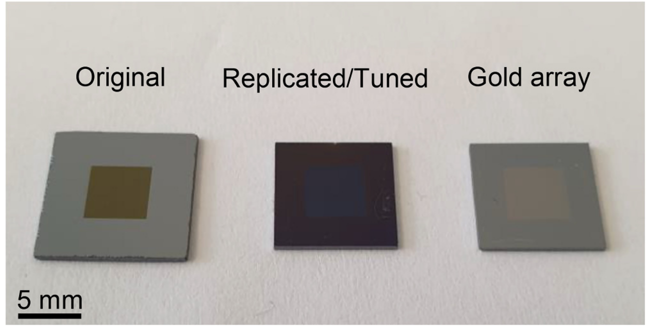

FIG. 2. Picture of the original stamp, a replicated and tuned stamp, and a gold nanoisland array fabricated with the tuned stamp. The patterned array for all stamps and samples is $5 \times 5\,\mathrm{mm}^2$.

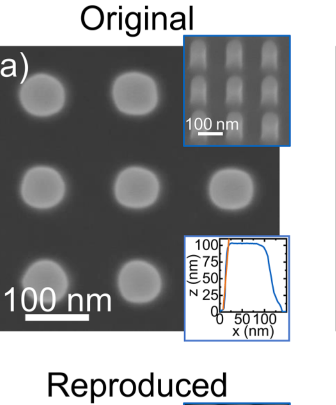

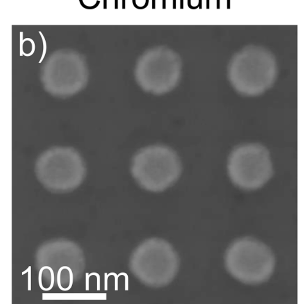

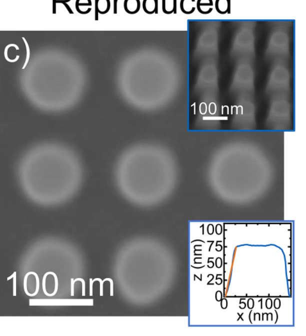

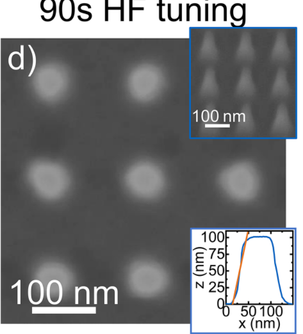

FIG. 3. SEM images of the stamp and replica at different times during the replication and tuning process: (a) The original stamp, (b) a chromium nanoisland array after LO-NIL, (c) a replicated stamp after dry etching and removal of the chromium, and (d) a tuned stamp after 90 s of HF tuning. For each stamp, the top and bottom insets present a 45° tilted SEM image of the stamp and an AFM height profile of a pillar of the stamp, respectively. The orange line in each AFM profile shows a linear fit to the sidewall of the respective pillar.

16 April 2024 08:25:33

of 45° and measured AFM height profiles of these stamps; both are shown in the respective insets. To evaluate the diameter of the features of our samples, we determine the diameter of several tens of individual features from the SEM images and calculate their mean value and standard deviation, which is given in parenthesis after each value. We measure a diameter of 74(1) and 73(2) nm for the original stamp and the chromium islands, respectively. Hence, the dimensions of the stamp are well preserved during the LO-NIL process and the chromium islands are an optimal hard mask for the further etching step. With a measured diameter of 99(3) nm, the pillars of the reproduced stamp are larger compared to the pillars of the original stamp. As the chromium nanoislands have no increased diameter, the increase in pillar diameter occurs during the reproduction process. Furthermore, if we compare the tilted SEM images of the original stamp with the reproduced stamp, the sidewalls of the pillars of the original stamp have a high, almost vertical slope, whereas the sidewalls of the pillars of the reproduced stamp have a decreased slope. To further analyze the slope of the pillars, we fitted a linear fit to the sidewalls of the original and reproduced stamps in the AFM height profile. The linear fits, indicated by orange lines in the insets, give average slopes of 8.4 and

© Author(s) 2022

3.1 for the sidewalls of the original and the reproduced stamps, respectively. Hence, the slope of the sidewalls clearly decreases during the reproduction process. We attribute the increase in diameter and the decrease in the slope of the sidewalls to charging effects during the dry etching of the SiO_2 pillars. SiO_2 is an insulating material, and therefore, the charges in the chromium disks and the underlying SiO_2, which are introduced by the ions in the plasma, cannot be immediately neutralized. Hence, an electrical field originates from the charges in the chromium discs. This electric field deflects further incoming ions away from the chromium disks, which leads to the increase in SiO_2 pillar diameter during the etching process. As over time more charges accumulate in the chromium disc and the forming SiO_2 pillars, the deflection of the incoming ions increases. This effect leads to a conic shape of the pillars as their diameter increases with increasing etch depth. Nevertheless, the circular shape of the pillars is not affected during the reproduction process. Furthermore, the increase in diameter allows us the production of SiO_2 nanoimprinting stamps with a larger diameter, which increases the variety of our method. Figure 3(d) presents an SEM image of a stamp after an HF tuning of 90 s. After the tuning process, the diameter of the pillars of the stamp decreases to 62(2) nm. Also, the conic shape of the pillars is visible in the tilted SEM image and the linear fit to the sidewalls in the AFM height profile gives a slope of 3.2. Hence, the tuning process has no influence on the slope of the sidewalls. Note, that the different heights of the pillars of the reproduced and the tuned stamp originate from different etching times during the reproduction process and are not related to the tuning process. Overall, the whole reproduction and tuning process enables the tuning of the pillar diameter without changing the underlying circular shape of the pillars. Furthermore, we reproduced and tuned a stamp with 200 nm squares (Fig. S1 in the supplementary material). The HF tuning also preserved the quadratic shape of the 200 nm stamps. Therefore, the tuning method preserves straight edges and corners in addition to circular features, allowing our reproduction and tuning method to be applied to more complex geometries.

C. Tuning imprinting stamps to different sizes

In Sec. II B, we validate our reproduction and tuning method; now, we will compare stamps with different HF tuning times to the original stamp. Figures 4(a)–4(e) show SEM images of the original 75 nm stamp, a reproduced stamp, and tuned stamps after 30, 60, and 90 s HF tuning, respectively. Here, the respective image at the top gives an overview over the features of the respective stamp, and the bottom image shows a zoom-in on the features to evaluate the diameter of the features of the respective stamp. For better comparison of the SEM images of different stamps, we took the SEM image at a position where all stamps inherited a defect from the original stamp. This defect can be seen in the bottom right corner of the top image in Fig. 4(a) and is indicated by the blue frame. All overview SEM images are taken at the same position on each stamp marked by this defect. Focusing on the overview image of the original stamp, aside from the defect in the corner, there are no defects visible in the SEM image. The pillars of the original stamp are arranged periodically in a cubic lattice with a center-to-center distance (pitch) of 150 nm. The bottom image in Fig. 3(a) shows a zoom-in on the stamp features. The features have a measured diameter of 74(1) nm. Thus, the deviation of the individual pillars within the array is within nanometer precision. Using this original

16 April 2024 08:25:33

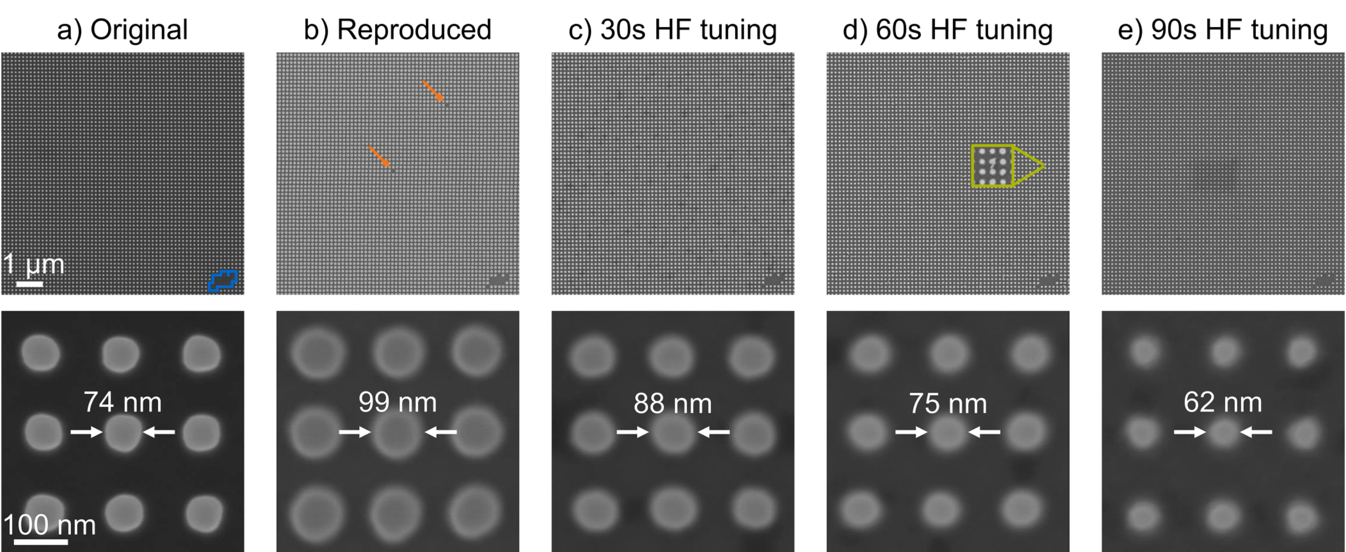

FIG. 4. SEM images of (a) the original stamp, (b) a reproduced SiO_2 stamp, (c) a SiO_2 stamp after 30 s HF tuning, (d) a SiO_2 stamp after 60 s HF tuning, and (e) a SiO_2 stamp after 90 s HF tuning. The respective top image shows an overview SEM image of each stamp at the same position on each stamp. The defect of the commercial stamp indicated by the blue frame is passed on to all other stamps. The bottom row shows a zoom onto the structures of each stamp. The diameter of the pillars are 74(1), 99(3), 88(3), 75(3), and 62(2) nm for the original stamp, the reproduced stamp, and the tuned stamps, respectively.

© Author(s) 2022

stamp, we performed the reproduction and tuning process described above to produce the SiO_2 stamps that are discussed in the following. Figure 4(b) shows SEM images of a reproduced stamp. Besides, the inherited defect in the lower right corner, we recognize two point defects in the top overview image marked by orange arrows, where at each site a single pillar is missing. However, we do not observe a systematic increase in defects in the SiO_2 stamps due to the reproduction method. To quantify the quality of our reproduced and tuned SiO_2 stamps, we introduce the yield of the process as the quotient between the number of functional pillars of the respective SiO_2 stamp and the number of pillars of the original. For the calculation of the yield, we use the overview images of Fig. 4 consisting of 4000 pillars. The yield for the reproduced stamp is 99.9%. For the pillars of the reproduced stamp, we measure a diameter of 99(3) nm. Therefore, the further HF tuning of the reproduced stamps starts at this pillar diameter. Besides the increased diameter, the pillars in the SEM image of the reproduced stamp are blurrier than the pillars of the original stamp. The increased blurriness of the images of the SiO_2 stamp arrives from the worse conductance of SiO_2 compared to silicon. Therefore, the electrons of the SEM are accumulating in the SiO_2, which influences the quality of the image, because the accumulated electrons deflect incoming and scattered electrons before they can hit the detector.

Next, we compare SiO_2 stamps after different HF tuning times. Figures 4(c), 3(d), and 3(e) show SEM images of three reproduced SiO_2 stamps after 30, 60, and 90 s of HF tuning, respectively. Again, the top images show overviews of the stamps with the inherited defect from the original stamp in the lower right corner of each image. For the 30 and 90 s tuned stamps, no further defects besides the inherited defect are visible in the overview SEM images. Therefore, the yield for the two SiO_2 stamps is 100.0%. In the SEM image of the 60 s tuned stamp, we find interconnections between some nanoislands. One of these interconnections is highlighted in the green framed zoom in Fig. 4(d). We attribute these interconnections to a defect during the chromium evaporation process. Excess chromium on the silicon surface leads to bridges between neighboring islands. Despite the defects, the yield of the 60 s tuned stamp is still at 96.9%. The SEM images below the overview SEM images show a closer look at the tuned SiO_2 pillars of the respective stamps. We measure pillar diameters of 88(3), 75(3), and 62(2) nm, after 30, 60, and 90 s of HF tuning, respectively. From the decrease in diameter, we calculate lateral etch rates of 0.18, 0.20, and 0.21 nm s^{-1}, respectively. The constant lateral etching rate allows us a precise adjustment of the pillar diameters within a few nanometers precision. Combining the precise etching with the reproducibility of the process (Table SI in the supplementary material) and the uniformity of the tuning process over the whole sample (Table SII in the supplementary material), both also within a few nanometers, we can produce stepless tuneable nanoimprinting stamps tailored for our experiments.

In this work, we focus on HF tuning times up to 90 s; as for smaller structures, our simulations show a decreased plasmonic response. Therefore, smaller structures are not sufficient for our plasmonic experiments. However, we fabricated additional stamps with longer HF tuning times to investigate the limits of our tuning process. Figure 5 shows SEM images of SiO_2 stamps after 120, 150, and 180 s HF tuning. The calculated diameters are 50(3), 37(3), and 29(2) nm for the shown stamps, respectively. We were not able to resolve smaller structures using our SEM. However, in theory, the limitation of the HF tuning process is the mechanical stability of the SiO_2 at the desired aspect ratio of the stamp pillars. For this work, we can state the feasibility of sub-30 nm stamp features.

a) 120s HF tuning

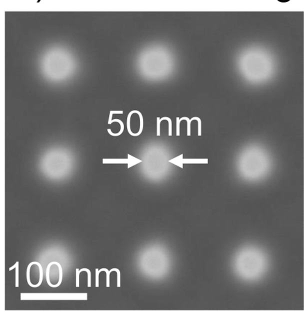

b) 150s HF tuning

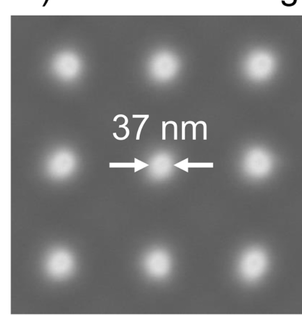

c) 180s HF tuning

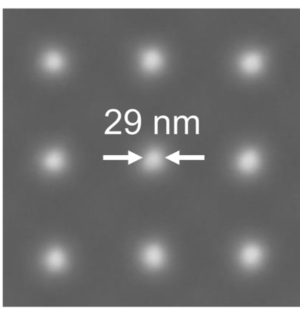

FIG. 5. SEM images of (a) a SiO_2 stamp after 120 s HF tuning, (b) a SiO_2 stamp after 150 s HF tuning, and (c) a SiO_2 stamp after 180 s HF tuning. The diameter of the pillars are 50(3), 37(3), and 29(2) nm for the tuned stamps, respectively.

16 April 2024 08:25:33

D. Fabrication of gold nanoisland arrays with the tuned stamps

For our experiments, we fabricate metal nanoisland arrays using LO-NIL. In the following, we discuss such nanoisland arrays produced with the stamps from Sec. II C. For the fabrication of the metal nanoisland arrays, we perform the LO-NIL process described in Figs. 1(a)–1(e). However, we also use the reproduced and tuned stamps and evaporate 17 nm gold with a 3 nm titanium adhesion layer instead of chromium. SEM images of these gold nanoisland arrays are shown in Fig. 6. Figures 6(a)–6(e) show each an overview on the top and a zoom in on the bottom of a gold nanoisland array fabricated with the respective stamps shown in Fig. 4. Additionally, beyond the SEM images of each nanoisland array, an AFM height profile of the respective array is presented. The SEM images in Fig. 6 show that it was possible to fabricate gold nanoisland arrays with all reproduced and tuned stamps and the AFM profiles show

© Author(s) 2022

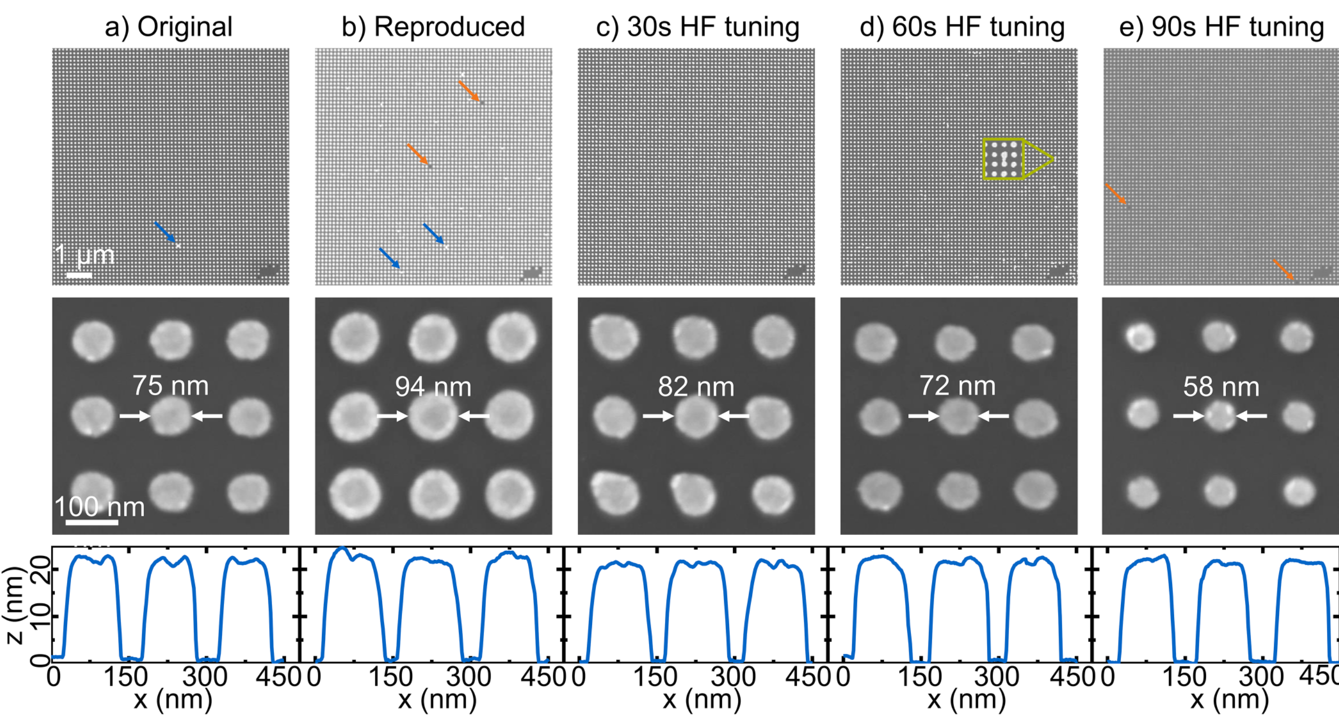

FIG. 6. SEM images of gold nanoisland arrays fabricated with (a) the original stamp, (b) a reproduced SiO_2 stamp, (c) a SiO_2 stamp after 30 s HF tuning, (d) a SiO_2 stamp after 60 s HF tuning, and (e) a SiO_2 stamp after 90 s HF tuning. The top row shows an overview SEM image of each sample at the same position on each array. The defect of the original stamp is visible in all nanoisland arrays. The second row shows a zoom onto the structures of each gold nanoisland array. The diameter of the gold nanoislands are 75(1), 94(3), 82(3), 72(4), and 58(3) nm for the original stamp, the reproduced stamp, and the tuned stamps, respectively. At the bottom, AFM height profiles are shown for each nanoisland array. The height of all nanoislands is 20(1) nm.

16 April 2024 08:25:33

that all gold nanoisland arrays have the same height of 20(1) nm. In the top SEM image of the nanoisland array fabricated with the original stamp (ORG array), we again recognize the defect inherited from the original stamp in the bottom right corner. Beside the inherited defect, a defect marked by a blue arrow is visible in the array; here, four nanoislands interconnect. This kind of defect originates from a collapse of four neighboring pillars in the working stamp. However, the LO-NIL process is not introducing systematic errors into the array. Again, we define a yield for the process, which is calculated from the overview images of Fig. 6. The yield for the LO-NIL process is the quotient between the number of functional gold nanoislands in an array divided by the number of pillars of the original stamp. The ORG array has a yield of 99.9%. The bottom image in Fig. 6(a) shows a zoom in on the individual nanoislands of the ORG array. The nanoislands of the ORG array have a diameter of 75(1) nm; hence, the LO-NIL method converts the dimensions from the stamp to the nanoisland array within nanometer precision. Next, we focus on the nanoisland array produced with the reproduced but not HF-tuned SiO_2 stamp (REP array). In the overview image at the top of Fig. 6(b), we find two different types of defects besides the inherited defect from the original stamp. The first type is a point defect where single nanoislands are missing marked by orange arrows. These defects are inherited from the reproduced stamp shown in Fig. 4(b). The second type examples marked by the blue arrows is an interconnection between two and four nanoislands like the defect in the ORG array. However, the LO-NIL process also worked for the reproduced stamp. The yield for the REP array is 99.2%. The zoom in at the bottom of Fig. 6(b) shows a closer look at the metal nanoislands. The fabricated gold nanoislands of the REP array have a measured diameter of 94(3) nm. Figures 6(c), 4(d), and 4(e) show the SEM images of the nanoislands produced with the 30 s HF-tuned stamp (30HF array), the 60 s HF-tuned stamp (60HF array), and the 90 s HF-tuned stamp (90HF array), respectively. In each overview SEM image, the inherited defect from the original stamp is visible. In the overview image of the 30HF array in Fig. 6(c), no further defects are present; hence, the yield is 100.0%. The zoom in shows circular nanoislands with a measured diameter of 82(3) nm for the 30HF array. In the overview SEM image of the 60HF array in Fig. 6(d), we recognize interconnections between some islands. These interconnection defects are inherited from the interconnection defects of the 60 s tuned stamp shown in Fig. 4(d). The green framed zoom shows the defect at the same position as in Fig. 4(d) for the 60 s tuned stamp. Despite these minor defects, the LO-NIL process produced a regular nanoisland array of circular disks with a process yield of 98.5%. The yield of the 60HF array increased compared

© Author(s) 2022

TABLE I. Diameter comparison of stamp pillars and nanoislands.

	Stamp pillars (nm)	Nanoislands (nm)	Difference (nm)
ORG	74(1)	75(1)	1(1)
REP	99(3)	94(3)	5(4)
30HF	88(3)	82(3)	6(4)
60HF	75(3)	72(4)	3(5)
90HF	62(2)	58(3)	4(3)

with the 60 s tuned stamp; hence, some defects from the stamp are corrected during the LO-NIL process. The nanoislands of the 60HF array have a diameter of 72(4) nm. Last, we investigate the 90HF array. In the overview SEM image of Fig. 6(e), we recognize two point defects besides the inherited defect. These two point defects are not visible in the SEM image of the tuned SiO_2 stamp in Fig. 4(e). Therefore, the defects are introduced during the fabrication of the working stamps from the tuned stamp or the LO-NIL process. The yield of the 90HF array is 99.9%. Therefore, we can state that despite the reproduction process as well as the LO-NIL process can introduce point defects into the nano arrays, the yield of the final gold nanoislands is hardly influenced by the processes. The zoom in on the gold nanoislands of the 90HF array at the bottom of Fig. 6(e) shows circular nanoislands with a diameter of 58(3) nm.

All measured diameters of the imprinting stamps and the fabricated arrays as well as the difference in measured diameter between the pillars of the respective stamps and nanoislands of each array are depicted in Table I. The diameter of the pillars of the reproduced and tuned stamps is always larger than the diameter of the nanoislands of their respective gold nanoisland array. However, the difference in diameter between the gold nanoislands and their respective imprinting stamp pillars stays constant during the tuning process. As the diameter of the gold nanoislands of the ORG array matches the diameter of the pillars of the original stamp, the difference in diameter for the SiO_2 stamps and their respective nanoisland arrays stems not from the LO-NIL process itself. We rather account the difference in measured diameter to a measuring error regarding the diameter of the pillars of the SiO_2 stamps. In particular, the decreased slope of the sidewalls of the reproduced stamps together with the charging effects in the SiO_2 during SEM imaging leads to an overestimation of the diameter of the pillars of the SiO_2 stamps. Focusing on the second column of Table I, the deviation in diameter between individual nanoislands of the same array stays also constant during the tuning process. Hence, the tuning process has no influence on the uniformity of the gold nanoisland arrays.

E. Influence of the diameter on the plasmonic properties of the gold nanoisland arrays

For our experiments, it is especially interesting to analyze the plasmonic properties of the nanoimprinted metal nanoisland arrays. Therefore, to investigate the influence of the diameter tuning process on the plasmonic resonance of the gold nanoisland arrays, we conduct UV-VIS transmittance experiments. Therefore, we fabricate gold nanoisland arrays in the same way as in Sec. II D on fused silica, which is transparent in the UV-VIS regime. In Fig. 7(a), the transmittance spectra of five different gold nanoisland arrays fabricated with the five different stamps from Sec. II are displayed. The green dots show the transmittance spectrum of the

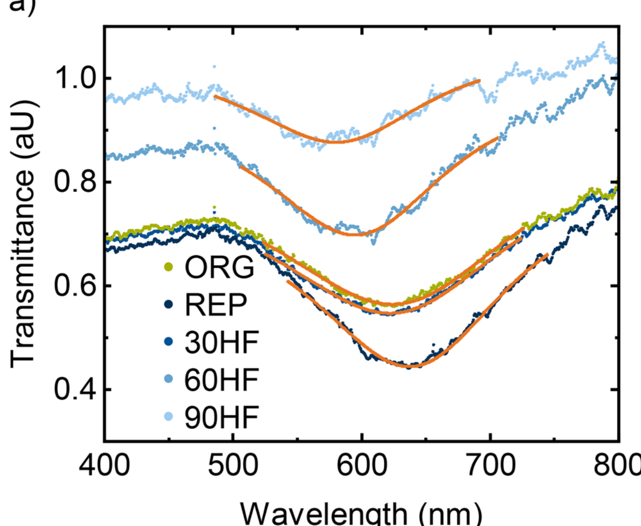

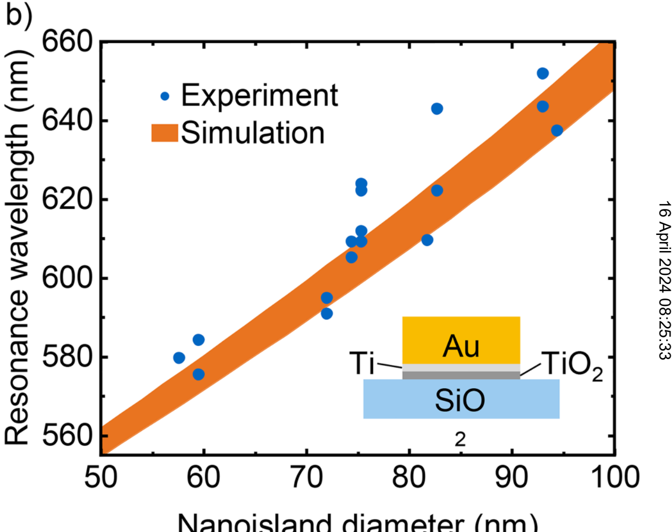

FIG. 7. (a) Transmittance spectra of the fabricated gold nanoisland arrays on fused silica. The green dots show the transmittance of the ORG array. The blue lines show the transmittance of the REP array, the 30HF array, the 60HF array, and the 90HF array from dark to light blue, respectively. The orange lines show a Breit–Wigner fit to each individual spectrum. (b) Comparison of the measured and simulated plamonic resonance wavelength. The blue dots represent the measured plasmonic resonance wavelength of our gold nanoisland arrays and the orange area represents the simulated plasmonic resonance wavelength for gold nanoisland arrays with a feature height of 20(1) nm. The orange area is obtained as the area between the simulations of a nanoisland array with 19 and 21 nm feature height. The inset shows a scheme of the simulated structures.

16 April 2024 08:25:33

© Author(s) 2022

ORG array and the blue dots show the transmittance spectrum of the REP array, the 30HF array, the 60HF array, and the 90HF array from dark to light blue, respectively. The transmittance spectrum of each measurement is normalized to the transmittance of the UV-VIS setup without a sample. In each plot, the orange line illustrates a Breit–Wigner fit to the respective spectrum. The fits are conducted to extract the plasmonic resonance wavelength from each measurement. The centers of the plasmonic resonance peeks lie at 609, 637, 609, 595, and 580 nm for the ORG array, the REP array, the 30HF array, the 60HF array, and the 90HF array, respectively. As expected from the literature,[6,22,23] the plasmonic resonance peak is blueshifted with decreasing gold nanoisland diameter as the localized plasmon resonance is confined in a smaller structure. The overall normalized transmittance increases with decreasing nanoisland diameter. The increase in transmittance can be explained by the decrease in overall gold on the sample surface with decreasing diameter of the gold nanoislands as the pitch of the nanoislands stays constant.

To compare our measurements with theory, we conducted simulations of our system. Figure 7(b) shows a comparison of the experimentally measured resonance wavelengths of gold nanoisland arrays with simulated plasmonic resonances. The blue circles represent the experimentally measured plasmonic resonance wavelengths of our samples plotted against the measured diameter of the nanoislands. The orange area shows the simulated plasmonic resonance wavelengths of gold nanoisland arrays on fused silica as a function of different nanoisland diameters for nanoisland heights of 20(1) nm. Hereby, the orange area arises from the area between the simulated transmittance spectrum of a nanoisland array with a feature height of 19 nm and an array with a feature height of 21 nm. In the simulations, the transmittance of a periodic array of gold nanoislands on fused silica is simulated. Our gold nanoislands on fused silica are represented by an SiO_2 substrate, a 3 nm titanium adhesion layer, which is half oxidized to TiO_2, and a gold layer of 17(1) nm. A scheme of the simulated stack is depicted in the inset of Fig. 7(b). As with the experimental data, the plasmonic resonance wavelength of the simulated arrays is extracted from simulated transmittance curves by fitting a Breit–Wigner function to the data. Focusing on the measured plasmonic resonance wavelengths, slight deviations in resonance wavelength between samples with the same measured diameter are present. We attribute the different resonance wavelengths to deviations in the evaporated metal height and different ratios of titanium and titanium oxide in the respective samples, which have an influence on the plasmonic resonance of the nanoislands. Overall, the measured plasmonic resonance wavelengths follow the simulated area for all nanoisland sizes. Hence, we can simulate the plasmonic response of the tuned system before we start the fabrication process to perfectly tailor the plasmonic system according to our experiments.

III. EXPERIMENTAL

A. Lift-off nanoimprint lithography process

All the following processes are carried out in a clean room. First, all substrates are cleaned in DMSO, acetone, and isopropanol for 7 min in an ultrasonic bath. Before the applications of the lift-off and imprint resist, the sample is heated to 250 °C for 1 min to remove residual water of the substrate surface. As lift-off resist, we use PGMI-SF6 diluted 1:2 with T Thinner from Kayaku Advanced Materials, USA. The lift-off resist is applied to the substrate surface via spincoating at 6000 rpm for 45 s, which leads to resist thickness of 41 nm. After application, the lift-off resist is baked at 250 °C for 3 min. As imprint resist, we use mr-I8020R diluted 1:1 with ma-T 1050 from micro resist technologies, Germany. The mr-I8020R is a thermo-viscous polymer with a glass transition temperature of 115 °C, which allows the later thermal imprinting. The imprint resist is also applied via spincoating and the rotation speed is adjusted to get the ideal thickness for each imprinting stamp to reduce the thickness of the forming residual layer. For the spinning time of 30 s, the thickness (rotation speed) of the imprint resist is 71 nm (4000 rpm) for the original stamp, 60 nm (5600 rpm) for the reproduced stamp, and 67 nm (4600 rpm) for the 30, 60, and 90 s tuned stamps. After application, the imprint resist is baked for 1 min at 100 °C.

For the imprinting process, we use semi-flexibel working stamps fabricated from OrmoStamp from micro resist technology, Germany. The working stamps are fabricated using the method developed by Mühlberger *et al.*[28] and adapted for our purposes by Nagel *et al.*[29] A working stamp is applied and the sample-stamp stack is imprinted in a Nano Imprinter from Obducat, Sweden. First, the stack is heated to 165 °C under a pressure of 5 bar. Then, the stack is imprinted at 165 °C under a pressure of 30 bar for 3 min. Still under pressure the stack is cooled to 90 °C and released afterward. Last, the working stamp is demolded mechanically.

For the removal of the residual layer, we use a RIE step in O_2 and C_4F_8 plasma inspired by the Bosch process for deep silicon etching,[30] where the C_4F_8 plasma forms long Teflon-like polymers to passivate the resist sidewalls, while the O_2 plasma etches the resist anisotropically in the z-direction. The RIE process is carried out in a Plasmalab 80 Plus from Oxford Instruments, UK with gas flows of 25 SCCM for O_2, 27 SCCM for C_4F_8, a chamber pressure of 30 mTorr, and an RF forward power of 200 W. Afterward, the lift-off layer is isotropically wet etched for 30 s using the developer AZ400K from Merck, Germany. To evaporate the metal, we use e-beam evaporation in a Pro Line PVD 75 system from the Kurt J. Lesker Company, USA. The deposition rates for the used metals are 1.2 Å s^{-1} for chromium and titanium and 2.0 Å s^{-1} for gold. We evaporate 20 nm of chromium for the metal hard mask during the reproduction process and 3 nm of titanium plus 15 nm of gold for the gold nanoisland arrays. Last, the lift-off is performed using in the remover m-Rem 700 from micro resist technologies, Germany in an ultrasonic bath at 50 °C for 3 min.

16 April 2024 08:25:33

B. Imprinting stamp replication and tuning

For the replication process, we first fabricate 20 nm thick chromium nanoislands on a silicon-SiO_2 substrate with a top layer of 200 nm thermal SiO_2 with the LO-NIL method described above. These nanoislands are used as hard mask in a subsequent anisotropic RIE etching process using O_2 and C_4F_8 plasma. Again, the forming polymers from the C_4F_8 plasma passivate the sidewalls, while the O_2 plasma etches the pillars in the z-direction. The RIE process is carried out in a PlasmaPro 80 Cobra from Oxford Instruments, UK with gas flows of 2 SCCM for O_2, 18 SCCM for

© Author(s) 2022

C_4F_8, a chamber pressure of 13 mTorr, an RF forward power of 100 W, and an ICP power of 150 W. After the RIE step, the chromium is removed with a chromium etch from Merck, Germany. Finally, the stamps are isotropically etched in 2% buffered hydrofluoric acid solution from Technic, USA. The etching process is performed under fume hood at room temperature. To ensure a constant HF acid concentration at the surface, the sample is constantly moved through the etching solution.

C. Imaging and image evaluation

All SEM images are taken with an Nvision 40 FIB/SEM from Zeiss, Germany. We use an aperture of 30 μm and an extraction voltage of 5 kV. For diameter evaluation, images at a magnification of 100 k are taken to measure the diameter of the pillars or nanoislands precisely. We use a self-developed graphical evaluation script to get the diameter of each pillar or nanoisland and calculate the mean value and standard deviation from those diameters.

The AFM images are taken with a Dimension Icon AFM in ScanAsystMode using ScanAsyst-Air AFM tips from Bruker, USA. The height profiles are extracted from these images. Afterward, the height profiles are tilt corrected and set to zero height at the lowest point.

D. UV-VIS measurements

For the UV-VIS measurement, we use a deuterium halogen light source AVA AvaLight-DH-S-BAL and an AvaSpec-2048 spectrometer from Avantes, Netherlands. To calculate the transmittance, we obtain a reference measurement of the setup without sample and a dark measurement of the setup without sample and illumination. The transmittance is calculated by dividing the measured spectrum subtracted by the dark measurement by the reference spectrum subtracted by the dark measurement. The plasmonic resonance wavelength is then evaluated by fitting a Breit–Wigner function to the plasmonic peak in each transmission spectrum.

E. Simulations

The simulations of the transmittance of our system are performed with COMSOL Multiphysics using the Electromagnetic Waves Module. We simulated the transmittance of each configuration for a wavelength between 50 and 100 nm in steps of 2 nm. To represent our gold nanoisland arrays, we simulate one nanoisland with periodic boundary conditions. The respective refractive indices for the simulation for the used materials air,[31] gold,[32] titanium,[33] titanium dioxide,[34] and silicon dioxide[35] are taken from the literature. To extract the simulated plasmonic resonance wavelength, we also fit a Breit–Wigner function to the simulated transmittance spectra.

IV. CONCLUSION

With our developed nanoimprint stamp reproduction and tuning method, we can alter the dimensions of imprinting stamp features of e-beam-fabricated imprinting stamps. We can tune the diameter of the imprinting stamp pillars and, therefore, the diameters of the nanoislands in the final metal nanoisland arrays fabricated with the tuned stamps by varying the etching time during the HF tuning step of our process. As the reproduction procedure enlarges the diameter of the imprinting stamp pillars, we are able to fabricate nanoislands with larger and with smaller diameters down to below 30 nm. The reproduction and the tuning process introduce no systematic defects into the imprinting stamp pillar arrays. Therefore, despite individual point defects, the reproduction and tuning process are not affecting the yield of our LO-NIL processes. After the tuning process, we can fabricate gold nanoisland arrays using the tuned stamps on various substrates. The diameter tuning of the gold nanoislands influences their plasmonic properties as expected, as the plasmonic resonance wavelength is blueshifted with decreasing gold nanoisland diameter. Furthermore, transmittance measurements show a good overlap between the simulated transmittance of our nanoislands and their measured transmittance. Hence, we are now able to tune the plasmonic response of our samples according to each experiment and application. If an experiment requires a certain plasmonic resonance wavelength, we can first perform a simulation to find the optimal dimensions for our nanoislands and then use the reproduction and tuning method to tailor a nanoimprinting stamp according to these simulations. Also, during the evaporation process of the LO-NIL process, we can adjust the thickness of our nanoislands. Combined with the possibility to tune the diameter of our nanoislands, we are now able to control the size of the nanoislands in all three dimensions. Thus, the reproduction and tuning process enables us to produce the optimal structures for each experiment, without the need to produce a new imprinting stamp in an expensive and time-consuming e-beam lithography process. Overall, we introduced a non-linear scalable method to stepless tune the feature sizes of nanoimprinting stamps below 30 nm without complex equipment in a cost-effective and simple process. Therefore, our method complements the various existing methods to fabricate and manipulate nanoimprinting stamps (Table SIII in the supplementary material) and further enhances the flexibility of nanoimprint lithography.

16 April 2024 08:25:33

SUPPLEMENTARY MATERIAL

See the supplementary material for reproducibility and uniformity studies, the tuning of 200 nm stamps, and the comparison of our process to other methods.

ACKNOWLEDGMENTS

We would like to acknowledge the support of the Central Electronics and Information Technology Laboratory—ZEIT^{lab}. This work was supported by Deutsche Forschungsgemeinschaft (DFG) through TUM International Graduate School of Science and Engineering (IGSSE), GSC 81. Furthermore, the authors thank the *Deutsche Forschungsgemeinschaft* (DFG, German Research Foundation) for funding (Project No. 245845833) within International Research Training Group IRTG 2022—Alberta Technical University of Munich School for Functional Hybrid Materials (ATUMS) and the "e-conversion" Cluster of Excellence (Grant No. EXC 2089/1-390776260), as well as the Bavarian State Ministry of Science and the Arts within the Collaborative Research Network "Solar Technologies go Hybrid (SolTech)".

© Author(s) 2022

AUTHOR DECLARATIONS

Conflict of Interest

The authors have no conflicts to disclose.

Ethics Approval

Ethics approval is not required.

DATA AVAILABILITY

The data that support the findings of this study are available from the corresponding author upon reasonable request.

REFERENCES

[1]S. Y. Chou, P. R. Krauss, and P. J. Renstrom, "Imprint of sub-25 nm vias and trenches in polymers," Appl. Phys. Lett. **67**, 3114 (1995).
[2]S. Y. Chou, "Nanoimprint lithography," J. Vac. Sci. Technol. B **14**, 4129 (1996).
[3]M. C. Traub, W. Longsine, and V. N. Truskett, "Advances in nanoimprint lithography," Annu. Rev. Chem. Biomol. Eng. **7**, 583–604 (2016).
[4]L. M. Cox, A. M. Martinez, A. K. Blevins, N. Sowan, Y. Ding, and C. N. Bowman, "Nanoimprint lithography: Emergent materials and methods of actuation," Nano Today **31**, 100838 (2020).
[5]B. D. Lucas, J. S. Kim, C. Chin, and L. J. Guo, "Nanoimprint lithography based approach for the fabrication of large-area, uniformly oriented plasmonic arrays," Adv. Mater. **20**, 1129–1134 (2008).
[6]R. D. Nagel, S. Filser, T. Zhang, A. Manzi, K. Schönleber, J. Lindsly, J. Zimmermann, T. L. Maier, G. Scarpa, K. Krischer, and P. Lugli, "Nanoimprint methods for the fabrication of macroscopic plasmonically active metal nanostructures," J. Appl. Phys. **121**, 084305 (2017).
[7]S. Filser, T. L. Maier, R. D. Nagel, W. Schindler, P. Lugli, M. Becherer, and K. Krischer, "Photoelectrochemical reactivity of well-defined mesoscale gold arrays on SiO_2/Si substrates in CO_2-saturated aqueous electrolyte," Electrochim. Acta **268**, 546–553 (2018).
[8]T. L. Maier, M. Golibrzuch, S. Mendisch, W. Schindler, M. Becherer, and K. Krischer, "Lateral silicon oxide/gold interfaces enhance the rate of electrochemical hydrogen evolution reaction in alkaline media," J. Chem. Phys. **152**, 154705 (2020).
[9]M.-S. Kim, J.-S. Kim, J. C. Cho, M. Shtein, L. J. Guo, and J. Kim, "Flexible conjugated polymer photovoltaic cells with controlled heterojunctions fabricated using nanoimprint lithography," Appl. Phys. Lett. **90**, 123113 (2007).
[10]M. G. Kang, M. S. Kim, J. Kim, and L. J. Guo, "Organic solar cells using nanoimprinted transparent metal electrodes," Adv. Mater. **20**, 4408–4413 (2008).
[11]L. J. Guo, "Nanoimprint lithography: Methods and material requirements," Adv. Mater. **19**, 495–513 (2007).
[12]S. Y. Chou, P. R. Krauss, W. Zhang, L. Guo and L. Zhuang, "Sub-10 nm imprint lithography and applications," J. Vac. Sci. Technol. B **15**(6), 2897–2904 (1997).
[13]K. Kemp and S. Wurm, "EUV lithography," C. R. Phys. **7**, 875–886 (2006).
[14]H. Namatsu, M. Nagase, K. Kurihara, K. Iwadate, T. Furuta, and K. Murase, "Fabrication of sub-10-nm silicon lines with minimum fluctuation," J. Vac. Sci. Technol. B **13**, 1473–1476 (1995).
[15]S. H. Ahn and L. J. Guo, "Large-area roll-to-roll and roll-to-plate nanoimprint lithography: A step toward high-throughput application of continuous nanoimprinting," ACS Nano **3**, 2304–2310 (2009).
[16]B. Heidari, I. Maximov, and L. Montelius, "Nanoimprint lithography at the 6 in. wafer scale," J. Vac. Sci. Technol. B **18**, 3557 (2000).
[17]Z. Yu, W. Wu, L. Chen, and S. Y. Chou, "Fabrication of large area 100 nm pitch grating by spatial frequency doubling and nanoimprint lithography for subwavelength optical applications," J. Vac. Sci. Technol. B **19**, 2816 (2001).
[18]Z. Yu and S. Y. Chou, "Triangular profile imprint molds in nanograting fabrication," Nano Lett. **4**, 341–344 (2004).
[19]Y. Yao, Y. Wang, H. Liu, Y. Li, B. Song, and W. Wu, "Line width tuning and smoothening for periodical grating fabrication in nanoimprint lithography," Appl. Phys. A **121**, 399–403 (2015).
[20]H. J. Park, M. G. Kang, and L. J. Guo, "Large area high density sub-20 nm SiO_2 nanostructures fabricated by block copolymer template for nanoimprint lithography," ACS Nano **3**, 2601–2608 (2009).
[21]S. Xiao, X. Yang, J. J. Hwu, K. Y. Lee, and D. Kuo, "A facile route to regular and nonregular dot arrays by integrating nanoimprint lithography with sphere-forming block copolymer directed self-assembly," J. Polym. Sci. Part B Polym. Phys. **52**, 361–367 (2014).
[22]K. S. Lee and M. A. El-Sayed, "Gold and silver nanoparticles in sensing and imaging: Sensitivity of plasmon response to size, shape, and metal composition," J. Phys. Chem. B **110**, 19220–19225 (2006).
[23]I. Zorić, B. Kasemo, C. Langhammer, and M. Zaaach, "Nanodisk plasmons: Material damping mechanisms," ACS Nano **5**, 2535–2546 (2011).
[24]C. Gao, Z. C. Xu, S. R. Deng, J. Wan, Y. Chen, R. Liu, E. Huq, and X. P. Qu, "Silicon nanowires by combined nanoimprint and angle deposition for gas sensing applications," Microelectron. Eng. **88**, 2100–2104 (2011).
[25]C. Pina-Hernandez, P. F. Fu, and L. J. Guo, "Ultrasmall structure fabrication via a facile size modification of nanoimprinted functional silsesquioxane features," ACS Nano **5**, 923–931 (2011).
[26]Q. Xia and S. Y. Chou, "Fabrication of sub-25 nm diameter pillar nanoimprint molds with smooth sidewalls using self-perfection by liquefaction and reactive ion etching," Nanotechnology **19**, 45 (2008).
[27]C. Wang, Q. Zhang, Y. Song, and S. Y. Chou, "Plasmonic bar-coupled dots-on-pillar cavity antenna with dual resonances for infrared absorption and sensing: Performance and nanoimprint fabrication," ACS Nano **8**, 2618–2624 (2014).
[28]M. Mühlberger, I. Bergmair, A. Klukowska, A. Kolander, H. Leichtfried, E. Platzgummer, H. Loeschner, C. Ebm, G. Grützner, and R. Schöftner, "UV-NIL with working stamps made from ormostamp," Microelectron. Eng. **86**, 691–693 (2009).
[29]R. D. Nagel, T. Haeberle, M. Schmidt, P. Lugli, and G. Scarpa, "Large area nano-transfer printing of sub-50-nm metal nanostructures using low-cost semi-flexible hybrid templates," Nanoscale Res. Lett. **11**, 562 (2016).
[30]F. Laermer, A. Schilp, and R. Bosch GmbH, "Method of anisotropically etching silicon," U.S. patent 5501893, US5501893A (1993).
[31]P. E. Ciddor, "Refractive index of air: New equations for the visible and near infrared," Appl. Opt. **35**, 1566–1573 (1996).
[32]R. L. Olmon, B. Slovick, T. W. Johnson, D. Shelton, S. H. Oh, G. D. Boreman, and M. B. Raschke, "Optical dielectric function of gold," Phys. Rev. B: Condens. Matter **86**, 285 (2012).
[33]P. B. Johnson and R. W. Christy, "Optical constants of transition metals," Phys. Rev. B **9**, 5056–5070 (1974).
[34]T. Siefke, S. Kroker, K. Pfeiffer, O. Puffky, K. Dietrich, D. Franta, I. Ohlídal, A. Szeghalmi, E. B. Kley, and A. Tünnermann, "Materials pushing the application limits of wire grid polarizers further into the deep ultraviolet spectral range," Adv. Opt. Mater. **4**, 1780–1786 (2016).
[35]L. Gao, R. Lemarchand, and M. Lequime, "Refractive index determination of SiO_2 layer in the UV/Vis/NIR range: Spectrophotometric reverse engineering on single and bi-layer designs," J. Eur. Opt. Soc. **8**, 13010 (2013).

16 April 2024 08:25:33

© Author(s) 2022